A suggested layout for the 7 long-baseline MeerKAT antennas.

I M Stewart

June 10, 2011

Abstract

Meerkat needs baselines of 20 km or more if it is to do good continuum work. The original plan to place 7 antennas (in addition to the central 64) along the 50 km access road to the core array, giving baselines of up to 50 km, now appears to be in doubt. Recently the SA SKA project called for proposals for placing the extra 7 antennas so as to give baselines up to 20 km. The present study proposes a layout in which the 7 dishes lie on a circle of 10 km radius from the array centre, but somewhat bunched along the East-West axis, so as to give a more even azimuthal coverage under typical conditions for commensal observing of the Chandra Deep Field South at dec = -27 degrees.

1 Introduction

The current design for Meerkat in which 64 antennas are distributed within a 4 km-radius circle, with a heavy concentration towards the centre, is optimized for HI work, in which the feasible targets are so close that they would be resolved over such (max 8 km) baselines. The continuum community, specifically the MIGHTEE collaboration, feared from an early stage that it would not be possible to do any worthwhile continuum science at L band with such a compact array - that at the sensitivity reachable by Meerkat, the density and size of continuum targets would mean that L-band continuum images would not only be unresolved but also heavily confused. This apprehension was confirmed in study I did last year (Stewart [2010]), for which an image created via the SKADS database (Wilman et al [2008]) was used as input.

Also at an early date, it was suggested that an extra 7 antennas on top of the central 64 (which I'll call the LB7 antennas, for brevity) could be arranged as a 'spur' along the access road, giving baselines up to about 50 km, albeit limited azimuthally to the approximately SE direction of the road. My study showed that these longer baselines indeed removed the confusion problem and allowed many of the sources in the input simulation to be resolved. At the declination of -27 degrees used in that study, the non-ideal azimuthal distribution of spur antennas dictated by the orientation of the access road gave rise to a very uneven azimuthal distribution of visibilities from these baselines, even with the use of earth-rotation aperture synthesis (ERAS) as well as wide-band multi-frequency synthesis (WBMFS). A new iterative tapering scheme (Stewart [2011]) allowed the best to be made of this and served to reduce the far-field sidelobes to a negligible level.

The necessity for the spur has lately been a subject of debate between the SA SKA project management and the MIGHTEE team. The latest suggestion (Horrell [2011]) has been to place an extra 7 antennas essentially anywhere but so as to provide baselines of no more than 20 km. Jasper Horrell called for detailed proposals obeying this criterion. The present report makes such a proposal.

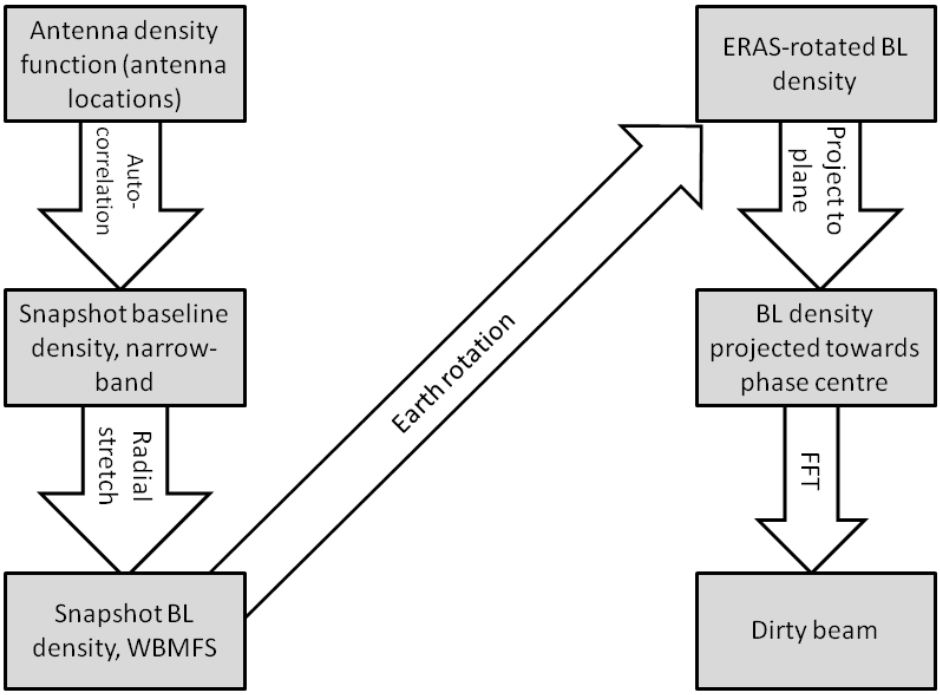


Figure 1: Block diagram showing the transforms required to convert antenna positions into a beam shape.

2 The proposed layout

As shown in figure 1, any attempt to optimize positions of array elements is complicated by the long chain of transforms between antenna positions and the synthesised beam and noise results.

Another problem is that desirable beam and noise criteria often conflict. Thus, it is desirable both to have low noise and low sidelobes: but the weighting of visibilities which gives the lowest noise, so-called 'natural' weighting, usually gives rise to significant power scattered into far sidelobes, due to irregularities in the density of visibility samples.

I have taken the approach that, for present purposes, a compact beam is more important than a low noise figure. Whereas high noise can (in principle at least) be defeated by longer observing times, it is difficult to squeeze high resolution from a low-resolution image.

One of the results of ERAS/WBMFS imaging is that the UV plane becomes very densely carpeted with visibility samples. It is then quite easy to grid the visibilities in such a fashion that, within the boundary imposed by the longest baselines, there are few or even no grid pixels which contain zero visibilities. That is certainly the case with the Meerkat core and, with care in placing of antennas, it can be made to be true also for the extra baselines to and between LB7 antennas. As my earlier study demonstrated, under such conditions of almost complete filling of the UV plane inside the boundary, judicious weighting of visibilities can do a great deal to reduce far-field sidelobes of the resulting 'dirty beam', which means less confusion and better dynamic range.

If one decides on an ideal visibility density profile then the antenna-placement issue becomes one of ensuring the 'natural' distribution of visibilities is as close to the ideal as possible. This is because the less one has to weight the natural visibilities to make them conform to the ideal, the less the noise RMS will depart from the natural-weighting optimum.

The ideal visibility density profile which results in a compact, low-sidelobes dirty beam will be essentially uniform, but tapered towards the boundary, with optionally some slowly-varying internal envelope. The weighted visibility 'image' must be smooth to avoid scattering power into sidelobes of the synthesized beam.

In considering where to place an extra 7 long-baseline antennas, it is useful to separate the various resulting baselines into three categories:

- 1596 in-in baselines, for which both antennas belong to the core.
- 21 out-out baselines, for which both antennas belong to the LB7.
- 399 in-out baselines, for which 1 antenna is core and the other LB7.

Since Justin Jonas (Jonas [2011]) has said that, whatever the final configuration of antennas, it was a firm proposal by SA SKA not to cross-correlate more than 64 at a time, I have assumed that only 57 core antennas will be active. That is the reason for the 1596 ($= [57 \times 56]/2$) baselines in the in-in group.

The in-in or core baselines give the highest sensitivity but are typically 1 km or less. The in-out or mid-length baselines are half as sensitive as core baselines but arguably about 10 km. The out-out baselines are low sensitivity (about 4.5 times lower again than the mid-length ones) but up to 20 km.

It seems to me that the in-out baselines give the best compromise between resolution and sensitivity and that early continuum science will probably be done using a weighting scheme which optimizes their measurements. In later years, if deeper observation of the same field are taken, it may then be thought desirable to re-weight the data to optimize the extra resolution obtainable via the out-out baselines. But I think the LB7 antenna positions should be chosen primarily with the in-out baselines in mind.

Working back through the flow chart in figure 1, an essentially uniform distribution of in-out baselines after a 24-hour ERAS implies a snapshot baseline density which (taking the inverse of the Abel transform of a 10-km radius pillbox function [see e.g. chapter 13 of Bracewell [2003]], then multiplying by u to counteract the increase in sample density towards

the rotation axis) has the (unnormalized) functional form

$$n(u,v) = u \left(1 - \frac{u^2+v^2}{10^2}\right)^{-0.5}. \quad (1)$$

This snapshot distribution is highly peaked towards the maximum length of 10 km for in-out baselines. Ideally we would then invert the WBMFS smearing, then the autocorrelation, to obtain a density distribution function for the extra antennas. However it may not be possible to do that and arrive at a real-valued function. It seems pretty clear to me that the closest one can approach this almost certainly unobtainable ideal is (as was suggested by Justin, [2011]) to place all the LB7 antennas on a 10-km radius circle.

Once the radii of the LB7 antennas are fixed, one has to look at the azimuths. Justin suggested an even azimuthal distribution, but I have chosen to bunch them towards the East-West axis. This accords better with the u proportionality of the ideal snapshot distribution of baselines shown in equation 1, and in practice it is found to give a more even baseline distribution after ERAS - which indeed was the point of the multiplication by u.

The azimuth angles (clockwise from north) chosen are -120, -75, -30, 45, 75, 110 and 135. These values were chosen 'by hand' to give a reasonably uniform distribution of in-out baselines.

3 Simulation results

3.1 Ground rules

The simulation conditions were chosen to facilitate comparison with the earlier study (Stewart [2010]). Briefly,

- The same SKADS image was used for input as in Stewart [2010].
- Perfect calibration was assumed.
- All sources were assumed to be flat-spectrum unpolarized.
- Distortions due to noncoplanarity were neglected.
- Far-field sources and all other effects of the primary beam were neglected.
- WBMFS/ERAS images were generated over a frequency band from 1.0 to 1.75 GHz and over an hour angle range of 12 hours, centred on the meridian (except where this pointed nearer to the horizon than the chosen minimum of 10 degrees.)
- Time samples were of length 100 s.
- For the in-in and in-out baselines:
  - The 750 MHz-wide band was broken into 10 channels of width 75 MHz.
- For the out-out baselines:
  - A 10-times finer frequency resolution was used for these baselines, so as to ensure continuous UV coverage at the gridding resolution employed. (The small number of baselines makes this computationally feasible.) The resulting gridded visibility images were then divided by 10 to make them consistent with those from other baseline sets.
- Zenith avoidance was neglected.
- Antenna shadowing was neglected.
- Image dimensions were 2048×2048 pixels.
- Sky pixel sizes were 0.1 arcsec, giving a UV grid pixel size of about 1007 waves.
- The simplest possible gridding scheme was employed, namely simply to add together the values located in each UV pixel.

- Noise figures were calculated for a 1000-hour observation.

The input SKADS image is shown in figure 2. For the sake of reference, the FTU-weighted image from last year's study (the bottom right panel of figure 5 of Stewart [2010]) is reproduced in figure 3.

3.2 At the CDF(S)

The Chandra Deep Field South is at RA = 53.11667 deg, dec = -27.80833 deg. It is the proposed site of the LADUMA deep field and, since MIGHTEE has been directed to observe commensally with LADUMA, perforce also the target for MIGHTEE. At this declination the telescopes can track from minus to plus 6 hr HA without exceeding the chosen horizon proximity limit of 10 degrees.

Figure 4 shows the natural distribution of sample density at this dec with 12 hour ERAS and 1.0-1.75 GHz WBMFS. The same density image is shown at two different brightness scales, to bring out the density distributions of the out-out and in-out baselines respectively. Note the (approx 50%) deficit between radii 22 and 32 (pixels). This can't be cured without significantly increasing the fractional bandwidth. Otherwise the in-out distribution is pleasingly uniform. Since the antenna positions were optimized to smooth the in-out rather than the out-out distributions, it is not surprising that the latter are not so good. But as remarked earlier, there seems little point in striving for maximum sensitivity with only 21 baselines.

Two ideal sample density distributions were employed. For both, an artificial distribution for the in-in plus in-out baselines was added to the natural distribution for the out-out baselines.

3.2.1 Tapered pillbox profile

The artificial profile had the mathematical form

$$P(r) = A\left(1 - \frac{r'}{r_0}\right)^p \tag{2}$$

where

$$r' = \frac{r}{1 - 2w(1-r)}. \tag{3}$$

I chose $A = 600$, $r_0 = 65$ pixels, $p = 3.2$ and $w = -1.3$. These values were chosen 'by hand' to give an acceptable fit between the profile and the in-out edge of the natural density. P is compared to a radial histogram of the natural density in figure 5.

After the out-out baselines were added to P, the expected RMS image noise was calculated for the visibility weights required to achieve the resulting density. The ratio between this and the RMS for natural weighting was 1.873, which reflects the low weighting given to the densely-packed samples toward the array core. Total calculated RMS noise for a 1000 hour observation was 0.508 μJy; an equivalent example pure-noise image had a measured noise RMS of 0.44 μJy. These two figures ought to be the same, but considering the rough-and-ready nature of the simulations I am fairly happy with agreement within 15%.

The dirty image (plus appropriate noise values) from applying this weighting to the SKADS input is shown in figure 6.

3.2.2 Profile which attempted to match the in-in baselines

For this profile, a P profile similar to that used in the preceding section (equations 2 and 3) was multiplied by a Q given by

$$Q(r) = \frac{1}{1/c + (r_1/r)^q}.$$

(This Q is essentially a broken power-law with the lower power set to zero.) I chose the following parameter values:

- $c = 1200$
- $r_1 = 80$
- $q = -2$
- $A = 143$
- $r_0 = 65$
- $p = 2$
- $w = -1$

PQ is compared to a radial histogram of the natural density in figure 7.

After the out-out baselines were added to PQ, the expected RMS image noise was calculated for the visibility weights required to achieve the resulting density. The ratio between this and the RMS for natural weighting was 1.157. Total calculated RMS noise for a 1000 hour observation was 0.314 μJy; an equivalent example pure-noise image had a measured noise RMS of 0.236 μJy.

The dirty image (plus appropriate noise values) from applying this weighting to the SKADS input is shown in figure 8. Note that it is heavily confused.

3.3 Other declinations

Baseline distributions corresponding to a pointing declination of +10 and -50 are displayed in figures 9 and 10. Note that, for the sake of clarity, the in-in baselines have not been included.

4 Conclusions

Positions for 7 extra 'long-baseline' dishes for Meerkat are proposed in this report. These were chosen to provide as smooth as possible distribution of visibility samples for baselines of 10 km or less, formed between the LB7 antennas and core antennas. Simulations were performed to investigate the imaging properties of the proposed layout under a number of different weighting schemes. The importance of concentrating on the LB7-core baselines was demonstrated. It seems likely that useful continuum science can be obtained from the proposed layout, for commensal observations of the Chandra Deep Field (South) with LADUMA.

References

[2003] Bracewell R. N. 2003 "The Fourier Transform and its Applications", McGraw-Hill, 3rd edition.

[2011] Horrell J. 2011, email sent on 19 May 2011.

[2011] Jonas J. 2011, email sent on 19 May 2011.

[2010] Stewart I. M. 2010, "MeerKAT core vs. core+spur: a comparison of image quality." http://www.ast.uct.ac.za/ ims/aufgaben/meerkat_spur.pdf

[2011] Stewart I. M. 2011, in preparation

[2008] Wilman R. J., Miller L., Jarvis M. J., Mauch T., Levrier F., Abdalla F. B., Rawlings S., Kloĉkner H.-R., Obreschkow D., Olteanu D. & Young S. 2008, MNRAS 388, 1335-1348

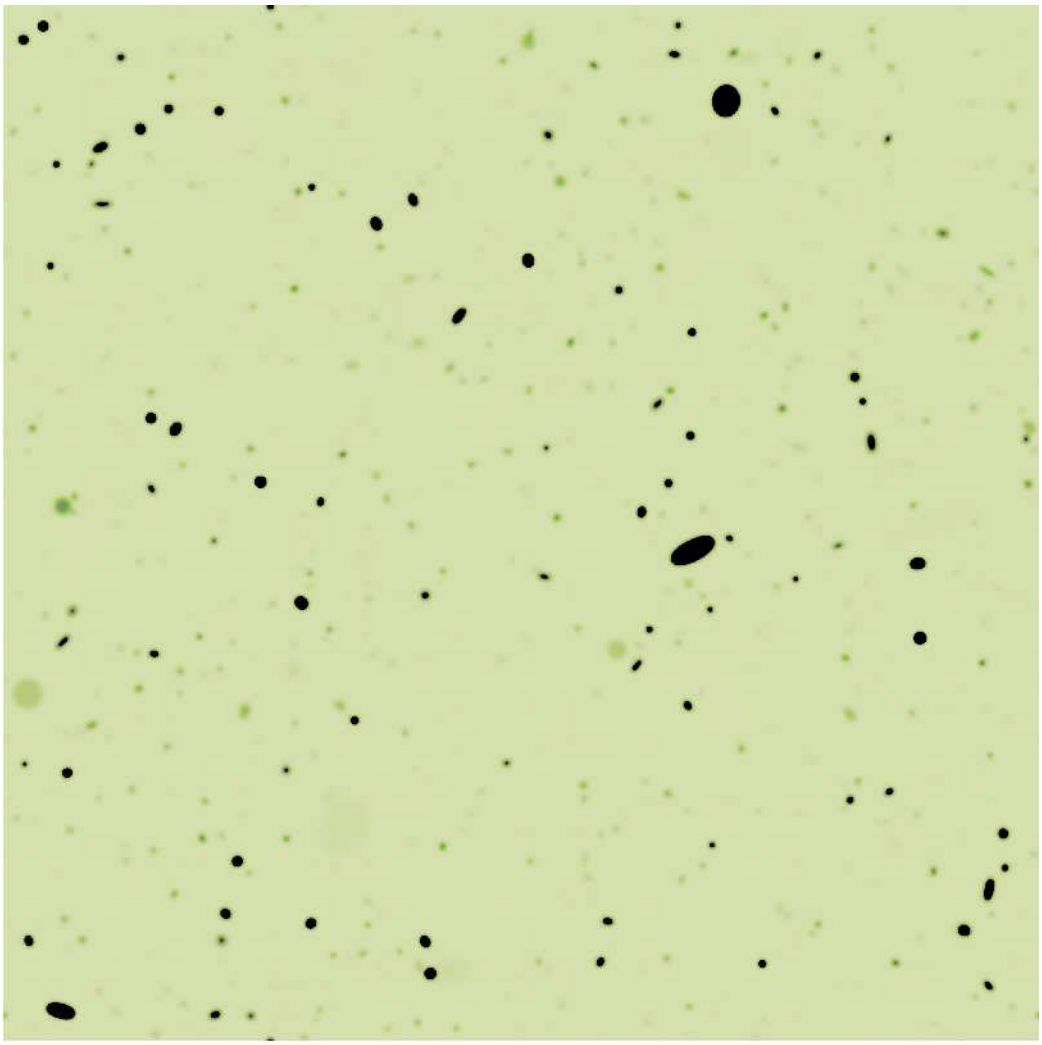


Figure 2: This is the input image for the simulation. It is a product of the SKADS database (Wilman et al [2008]). The same image was used in my previous study (Stewart [2010]). The image shown here (but not that used in the simulation) has been convolved with an 0.5-pixel-wide Gaussian to aid readability. The colour scale has been chosen such that a 2 μJy source begins to have a tint of purple.

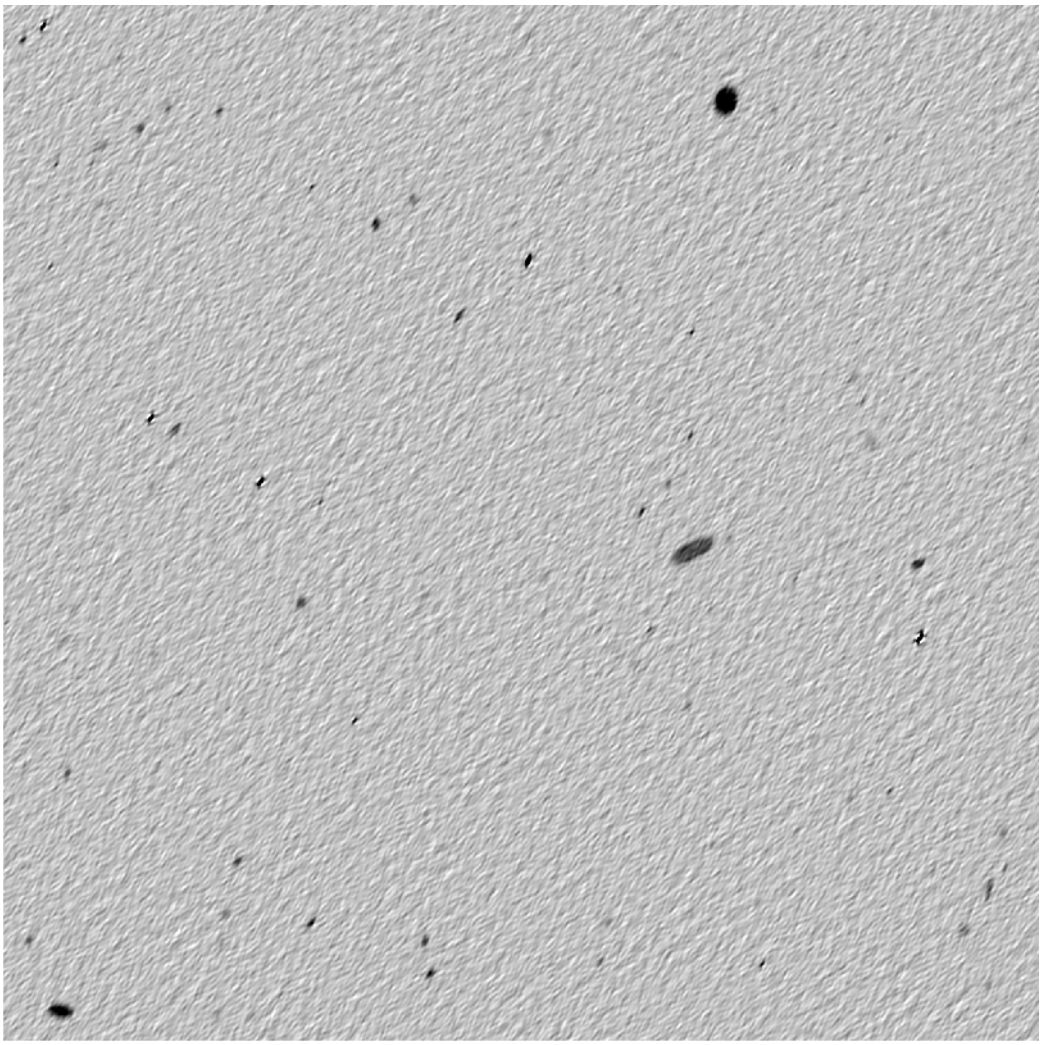


Figure 3: This was my 'best efforts' 1000-hour dirty image from the 2010 study of the characteristics of the original spur antennas (Stewart [2010]). A feathered-tapered weighting (Stewart [2011]) was employed to reduce sidelobes and maximize sensitivity. Sources down to about 2 μJy can be detected. Resolution is excellent.

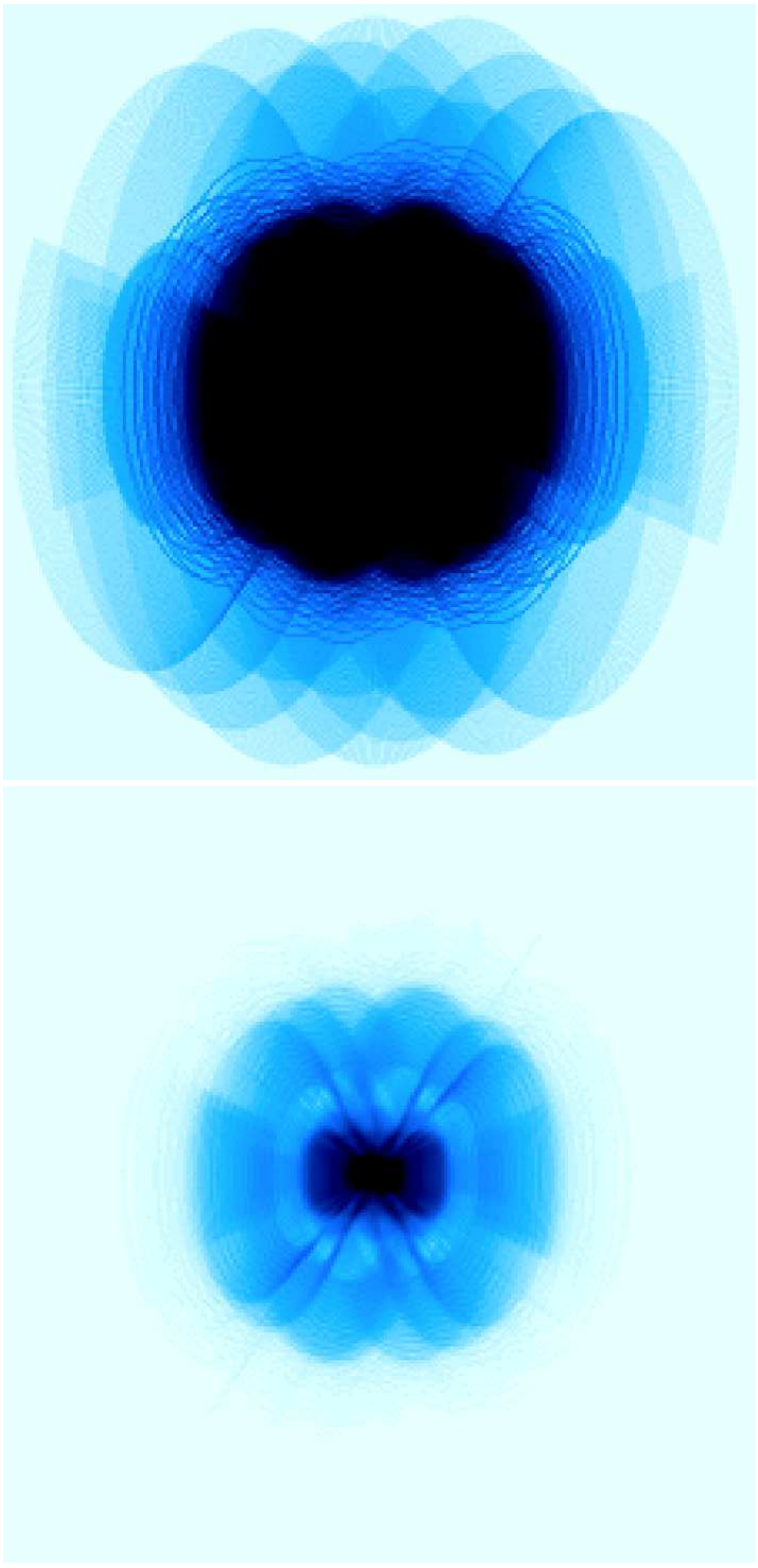


Figure 4: This figure shows two views of the same image. 'North' is to the left, 'West' is up. The image shows the visibility sample density obtained with the proposed LB7 layout, with 1.0 to 1.75 GHz wide-band multi-frequency synthesis and 12-hour Earth-rotation aperture synthesis, at a declination of -27 degrees. The upper pane has been made much more saturated in order to bring out the faint details of the out-out baselines (up to 20 km). The lower pane shows details of the in-out baselines (up to 10 km).

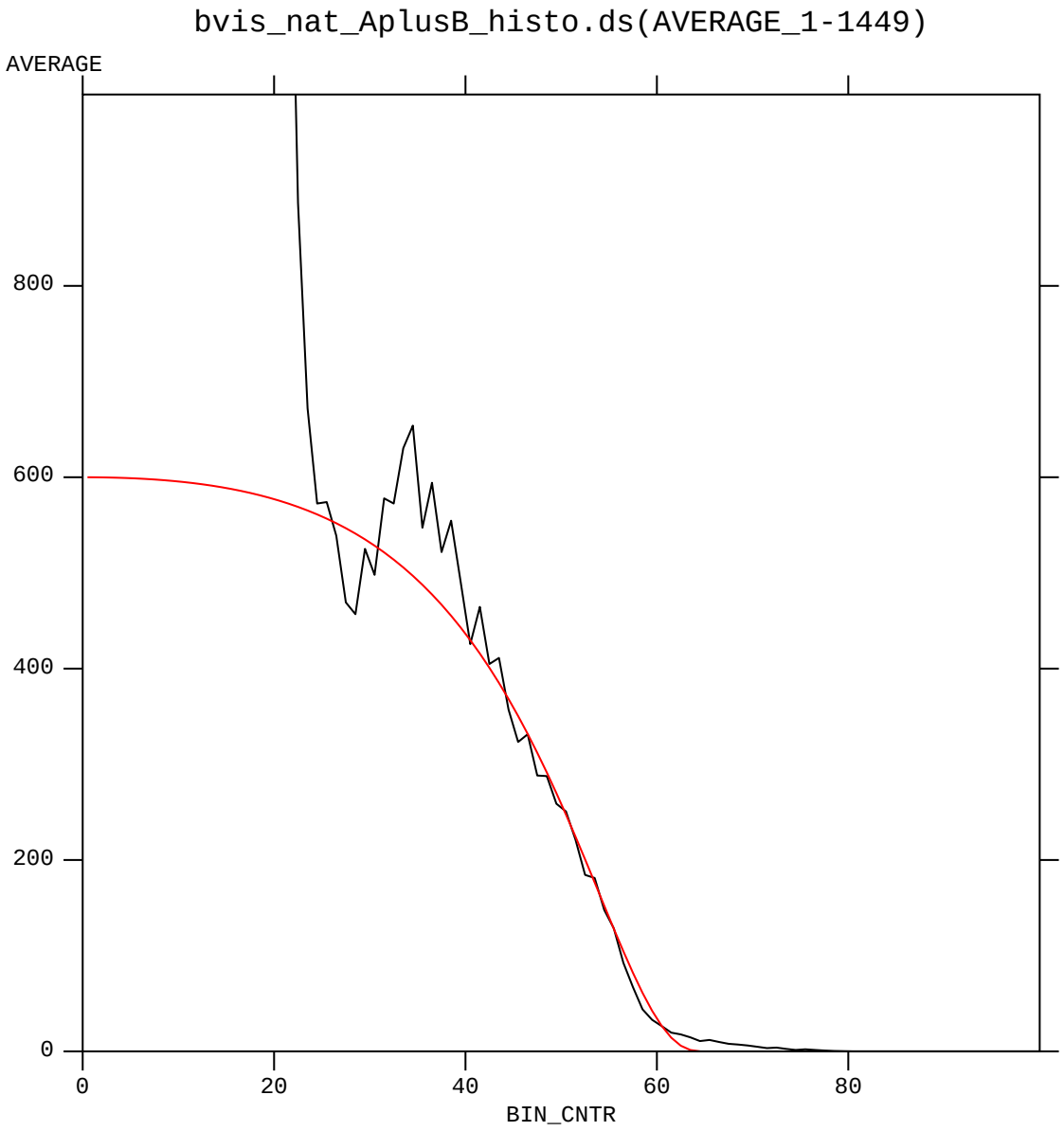


Figure 5: This shows the average density of visibility samples as a function of baseline radius. The X coordinate is in units of the UV plane gridding pixels, which are about 1007 waves wide. The black line shows the natural density at declination -27, with the WBMFS and ERAS parameters given in the body of the report. The red line shows the desired density profile, which is the 'tapered pillbox' mentioned in section 3.2.1.

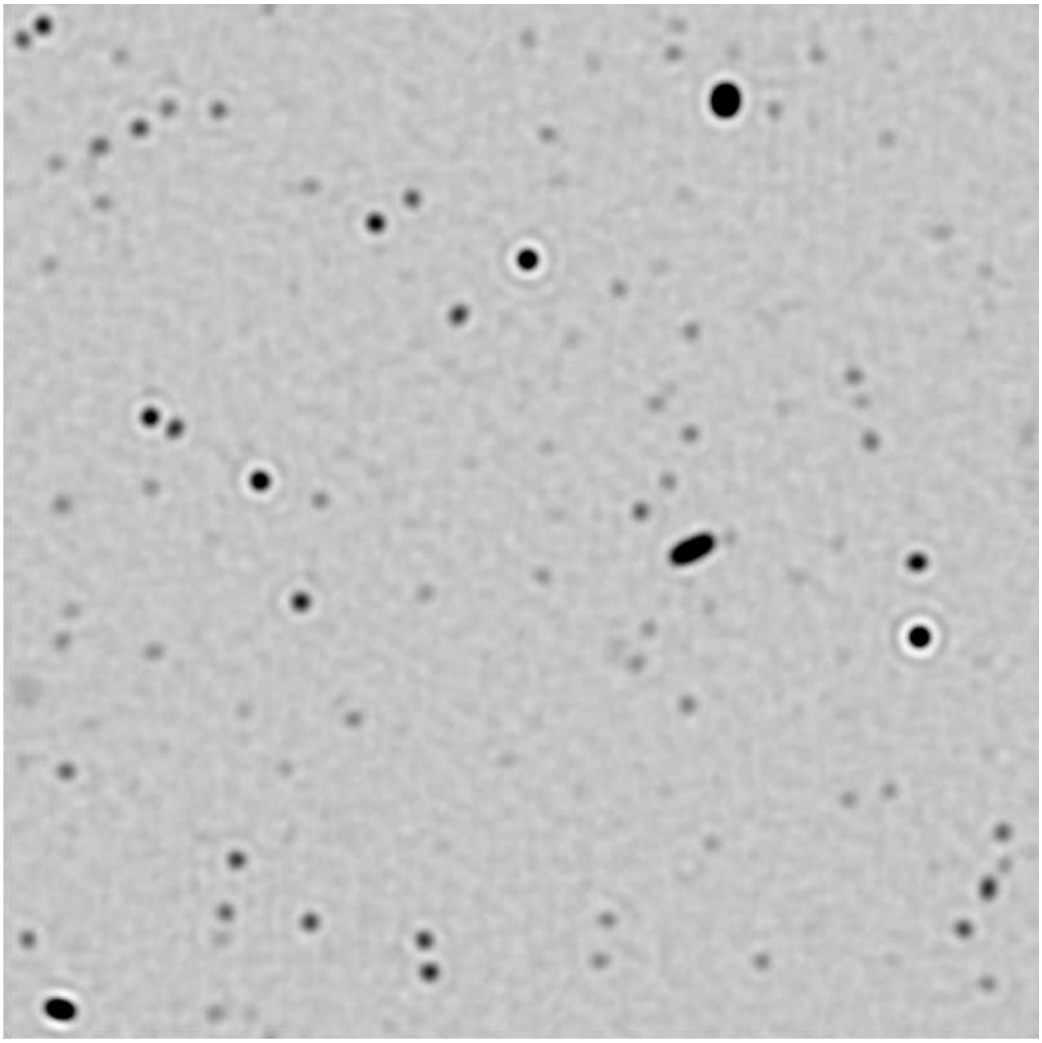


Figure 6: This shows the 1000-hour dirty image resulting from the 'tapered pillbox' profile mentioned in section 3.2.1. Sources down to about 2 μJy can be detected. The larger sources are resolved.

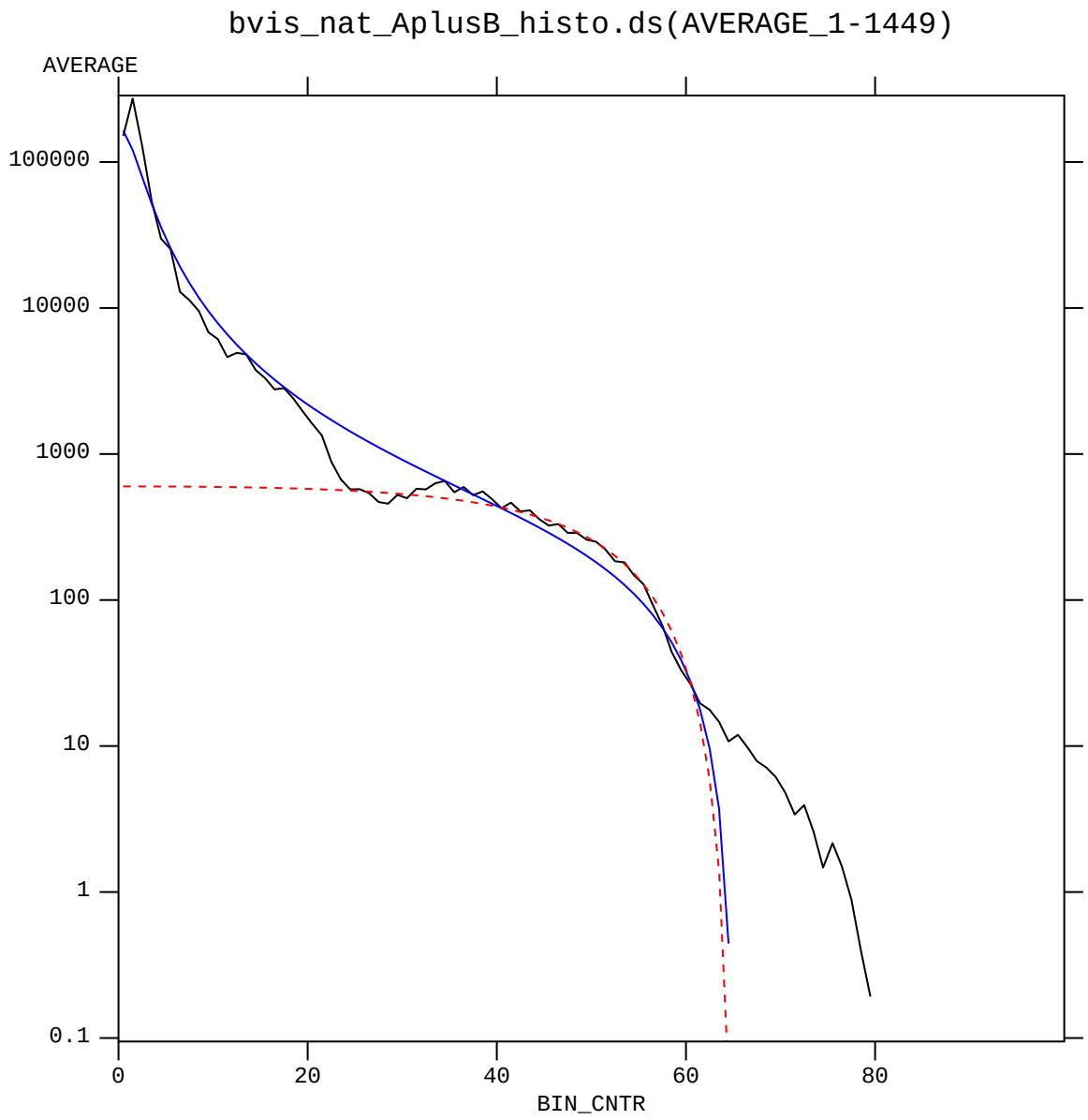


Figure 7: This is essentially the same plot as shown in figure 5, but the Y axis has now a log scale. The black line shows the natural density of samples as before; the blue line shows the desired density profile as described in section 3.2.2. The 'tapered pillbox' profile, shown by the dotted red curve, is included for comparison purposes.

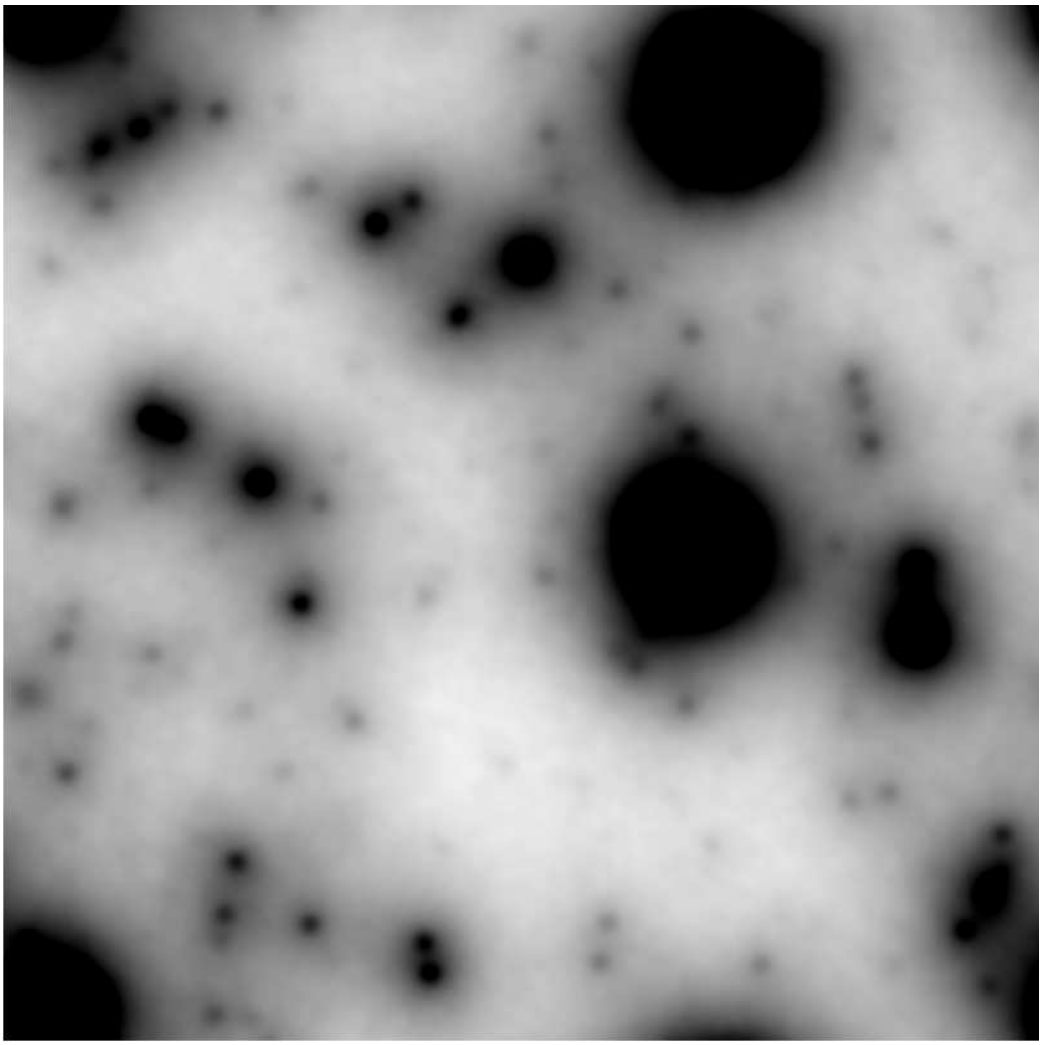


Figure 8: This shows the 1000-hour dirty image resulting from the high-sensitivity profile described in section 3.2.2. The extra sensitivity however is all at short baselines, for which confusion rather than thermal noise is the limiting factor at this depth.

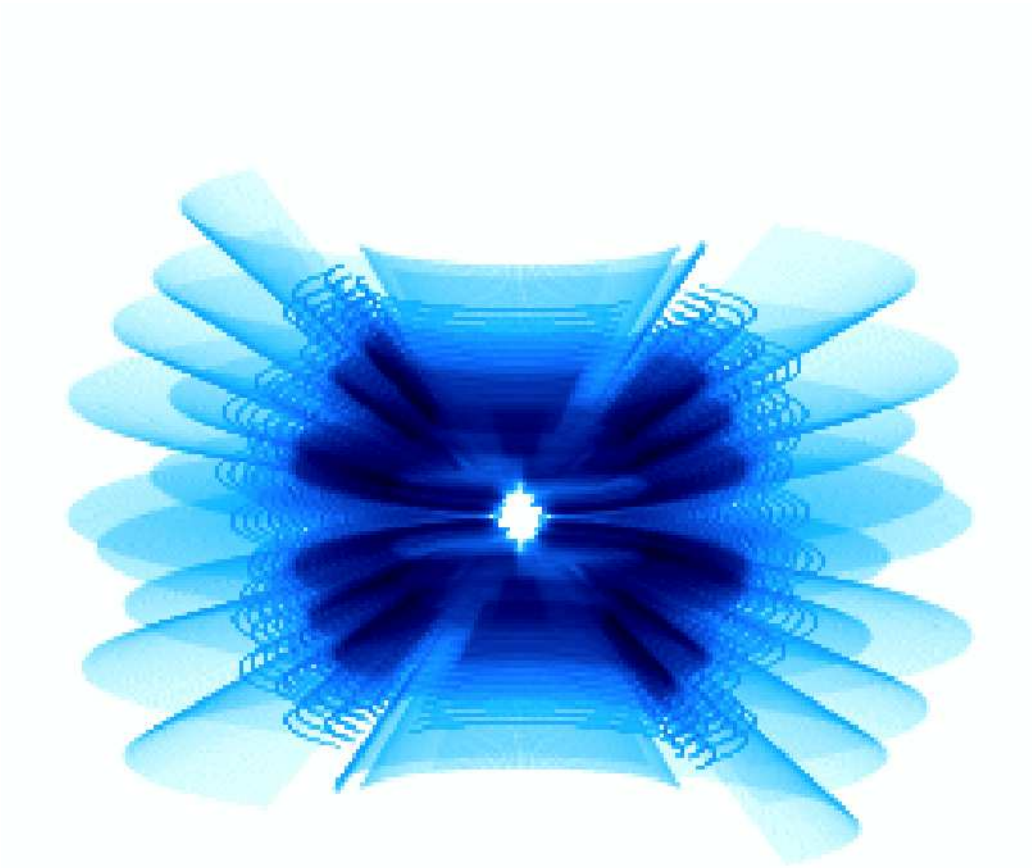


Figure 9: The density of visibility samples, for all but core-core baselines, at declination +10 degrees.

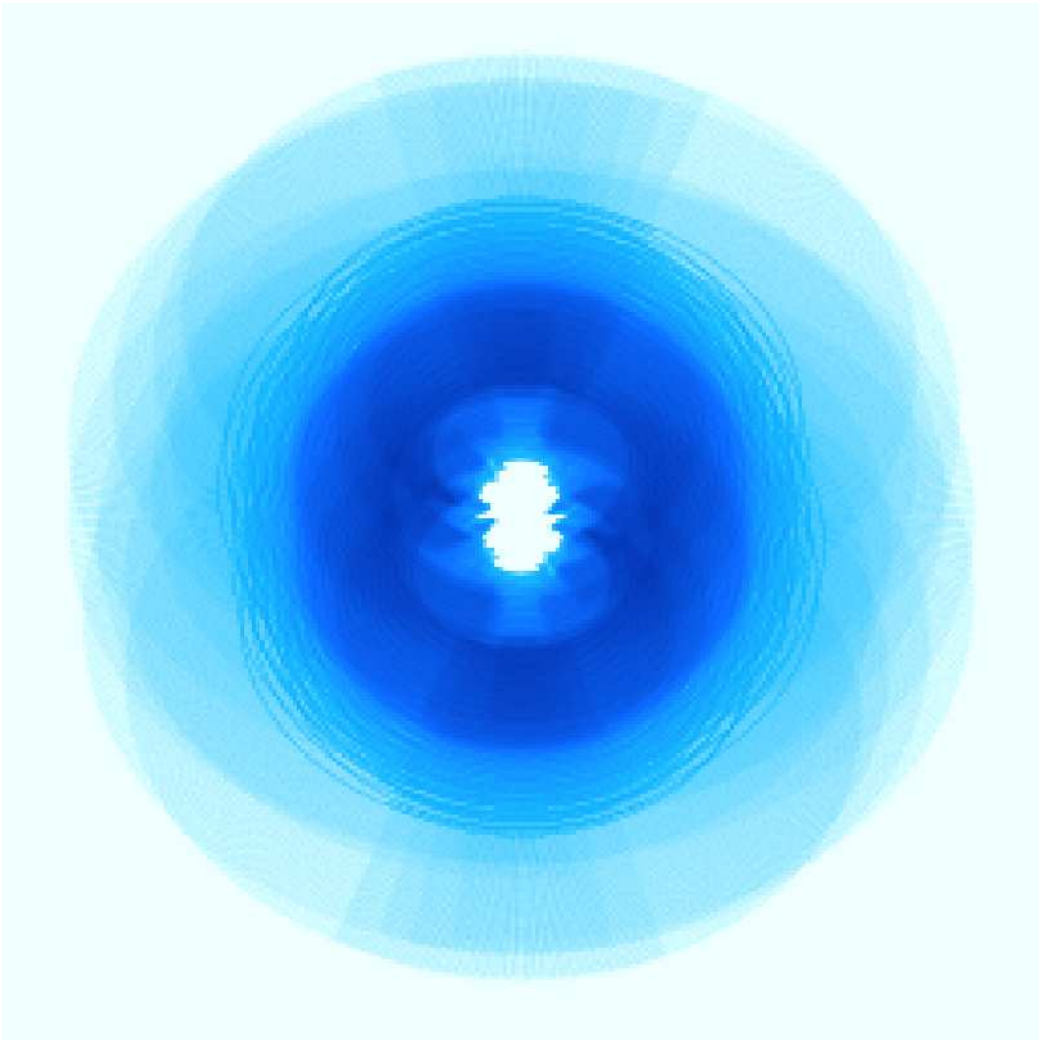


Figure 10: The density of visibility samples, for all but core-core baselines, at declination -50 degrees.